

Cooling in Primordial Structure Formation

U. Maio*, B. Ciardi*, K. Dolag* and L. Tornatore†

*Max-Planck-Institut für Astrophysik, Garching b. München, Germany

†Università di Trieste and INFN, Trieste, Italy

Abstract. Cooling is the main process leading to the condensation of gas in the dark matter potential wells. In a metal free environment, the main available coolants are H, He, H₂ and HD molecules; once the gas is enriched with metals, their contribution becomes dominant. Here, we present our implementation, in the Gadget2 code, of molecular and metal line cooling at the temperatures ($T < 10^4$ K) relevant for primordial structure formation.

Keywords: early universe; cosmology; theory; galaxies; formation

PACS: 98.62.Ai

INTRODUCTION

According to the most popular scenario of structure formation, cosmic objects form from in-fall of gas into dark matter potential wells. Only if radiative losses are sufficient to make the gas condense and fragment star formation can start. Thus, in order to understand the whole phenomenon, a detailed study of the chemical and cooling properties of baryonic matter is needed.

In the typical conditions of primordial structure formation, molecules are the only relevant coolants. Once the gas is enriched with metals, they give a stronger contribution. For these reasons, we have extended previous “non-equilibrium” calculations [1] in order to include, in the numerical code Gadget2 [2], the deuterium chemistry (see also [3, 4, 5, 6, 7]) and fine structure metal line cooling [8, 9, 10, 11].

In the following, we discuss the cooling of primordial and enriched gas and show the results of our tests about cosmic structure formation and cluster evolution; then, we present our conclusions.

COOLING

The cosmic medium has very low density (and thus is not in thermodynamic equilibrium) and low temperature. Therefore, we follow [for all the details and references, see 12] the non-equilibrium evolution of H, He and D chemistry (i.e. e⁻, H, H⁺, H⁻, He, He⁺, He⁺⁺, H₂, H₂⁺, D, D⁺, HD, HeH⁺); once the medium is enriched, we model the fine structure transitions of metals (C⁺, O, Si⁺, Fe⁺), which are relevant in the low temperature regime.

In Figure 1, we show the resulting cooling function, varying individual metal number fractions between 10^{-6} and 10^{-3} ; a hydrogen number density of unity and fractions of 10^{-5} and 10^{-8} for H₂ and HD respectively are

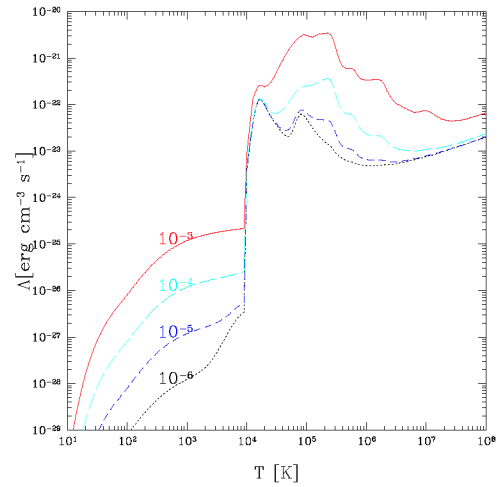


FIGURE 1. Cooling function computed with metal number fractions equal to 10^{-6} (black dotted line), 10^{-5} (blue short-dashed line), 10^{-4} (cyan long-dashed line), 10^{-3} (red solid line); a hydrogen number density of unity and fractions of 10^{-5} and 10^{-8} for H₂ and HD respectively are assumed.

assumed. The values for H₂ and HD molecules are fairly typical for the IGM gas at the mean density. The high temperature part of the plot (at $T \geq 10^4$ K) is obtained from the classical tables by [13].

Molecules

We test our implementation of primordial molecules in Gadget2 by running cosmological simulations of early structure formation (no metals); we adopt the concordance Λ CDM cosmology with $h = 0.7$, $\Omega_{0m} = 0.3$, $\Omega_{0b} = 0.04$, $\Omega_{0\Lambda} = 0.7$; the power spectrum is normalized assuming a mass variance in a $8\text{Mpc}/h$ radius

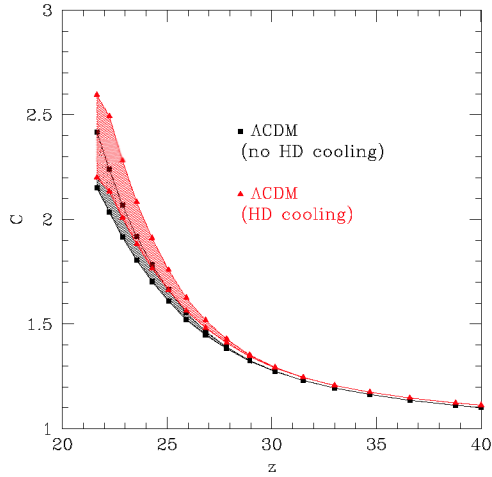


FIGURE 2. Gas clumping factor as a function of redshift in a Λ CDM cosmology with $h = 0.7$, $\Omega_{0M} = 0.3$, $\Omega_{0b} = 0.04$, $\Omega_{0\Lambda} = 0.7$, $\sigma_8 = 0.9$. The squares refer to the clumping factor computed with standard atomic line cooling and H_2 cooling, while the triangles refer to a case which includes also HD cooling. The shaded regions correspond to the variation of the maximum overdensity considered between 100 (lower line in both cases) and 500 (upper line in both cases).

sphere $\sigma_8 = 0.9$ and the spectral index is chosen to be $n = 1$. We sample the cosmological field (in a periodic box of 1 Mpc comoving side length) with 324^3 dark matter particles and the same number of gas particles, having a mass of about $1040 M_\odot$ and $160 M_\odot$, respectively. The comoving Plummer-equivalent gravitational softening length is fixed to 0.143 kpc. We include the main reactions involving H, He, H_2 and HD chemistry and compare the results with those of [14], whose Λ CDM simulations have the same features, but the chemical set does not follow the evolution of D, D^+ and HD and does not include H_2^+ cooling. To quantify the differences between the two runs and the efficiency of the HD cooling we calculate the gas clumping factor; for the sake of comparison, we calculate it using only particles with density below a given overdensity threshold, δ_M , and we make δ_M vary in the range [100, 500]. In Figure 2, we plot the clumping factor and in Figure 3, we show the temperature evolution maps of our simulation at different redshifts. The results show an increment (decrement) of about 10% in the clumpiness (temperature) of the gas when HD chemistry is included.

Metals

To test the implementation of metal cooling in the low temperature regime, we simulate the formation and

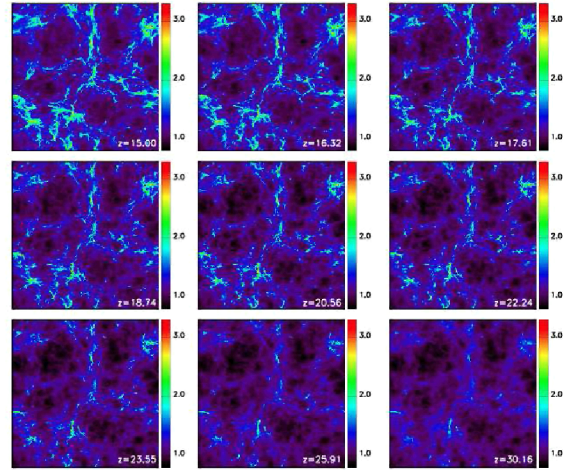


FIGURE 3. Temperature evolution maps between redshift 15 and ~ 30 for a Λ CDM cosmology with $h = 0.7$, $\Omega_{0M} = 0.3$, $\Omega_{0b} = 0.04$, $\Omega_{0\Lambda} = 0.7$, $\sigma_8 = 0.9$. The color bars refer to the decimal logarithm of the temperature in Kelvin. On the bottom right of each panel, the redshift is quoted.

evolution of a cluster (including metal pollution) and compare the results to a case without such cooling. The “zoomed initial condition technique” [15] is used to extract from a dark matter-only simulation with box size of 479 Mpc/h (we adopt a Λ CDM cosmology with $H_0 = 70 \text{ km s}^{-1} \text{ Mpc}^{-1}$, $\sigma_8 = 0.9$, $\Omega_{0\Lambda} = 0.7$, $\Omega_{0m} = 0.3$, $\Omega_{0b} = 0.04$) a smaller region and to re-simulate it at higher resolution introducing also gas particles. The cluster evolution is simulated with about $2 \cdot 10^5$ particles. The comoving Plummer-equivalent gravitational softening length is 5 kpc/h. At redshift zero, the selected cluster has a virial mass of about $10^{14} M_\odot/h$, a virial radius of about 1 Mpc/h and a virial temperature of $2 \cdot 10^7$ K. We start the simulation with no metallicity content. Then, the metal abundances are consistently derived following the star formation history of the system (see also [16]).

In Figures 4 and 5, we show phase spaces and cooling diagrams, respectively, for the outputs of the simulations at redshift $z = 0$. The color bar refers to the decimal logarithm of the cooling function, for Figure 4, and to the decimal logarithm of the gas density, for Figure 5.

On the left side, we plot the results referring to the high temperature cooling only case, while, on the right side, we plot the results obtained including also fine structure metal line cooling.

The main effect of our metal cooling implementation is to lower the temperature of the dense medium, generating the sharp triangular area visible in the $\rho - T$ space, on the right panel of Figure 4, at $T < 10^4$ K and $\rho > 10^{-26} \text{ g cm}^{-3}$. In the cooling diagrams (Figure 5), the area at high temperatures represents the hot, low density ICM. When the ICM starts to get denser, cooling gets

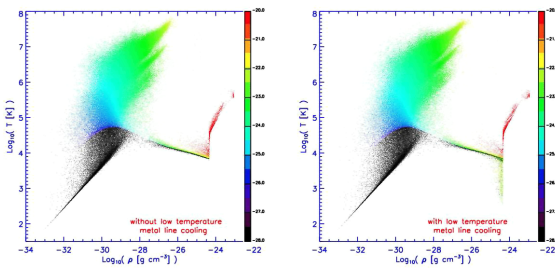


FIGURE 4. Phase diagrams for the particles of a cluster simulation (adopted parameters: $h = 0.7$, $\Omega_{0\Lambda} = 0.7$, $\Omega_{0m} = 0.3$, $\Omega_{0b} = 0.04$, $\sigma_8 = 0.9$). The left panel refers to the case when low temperature metal line cooling is not included, the right panel to the case when low temperature metal line cooling is included. The color bar gives the decimal logarithm of the cooling function (in c.g.s units).

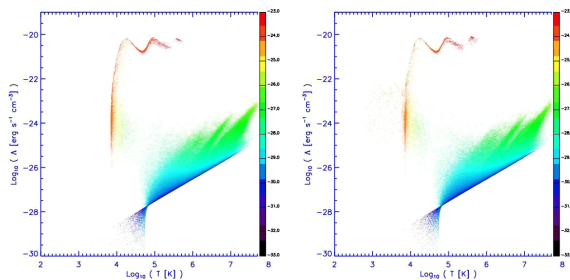


FIGURE 5. Cooling diagrams for the particles of a cluster simulation (adopted parameters: $h = 0.7$, $\Omega_{0\Lambda} = 0.7$, $\Omega_{0m} = 0.3$, $\Omega_{0b} = 0.04$, $\sigma_8 = 0.9$). The left panel refers to the case when low temperature metal line cooling is not included, the right panel to the case when low temperature metal line cooling is included. The color bar gives the decimal logarithm of the gas density (in c.g.s. units).

more efficient: the corresponding gas particles are represented by the points belonging to the upper branch of the cooling function and they are brought to lower and lower temperatures. Feedback from the star formation partially pushes some of them away from the cooling curve to slightly higher temperatures. Below 10^4 K, only particles which are metal enriched can further cool down, when metal line cooling is included (right panel of Figure 5). Metals are efficient in cooling polluted regions down to 10^2 K – 10^3 K.

CONCLUSIONS

We have presented time dependent calculations of the cooling properties of cosmic gas, using the contributions of several chemical species and we have tested the effects on cosmic structure evolution. Hydrogen derived molecules (like H_2 and HD) are effective in cooling

metal-free gas below a temperature of $\sim 10^4$ K, the typical temperature range of primordial objects. On the other hand, when the medium is polluted by material expelled from stars, metals are expected to become the main coolants. Therefore, we follow the evolution of e^- , H, H^+ , He, He^+ , He^{++} , H_2 , H_2^+ , H^- , D, D^+ , HD, HeH^+ , O, C^+ , Si^+ , Fe^+ .

We find that adding the deuterium chemistry and HD contribution to the cooling function in simulations of primordial structure formation results in a slightly higher clumping factor of the gas, i.e. clouds are denser and more compact, at high redshifts, with respect to the case when only H, He and H_2 cooling is considered (even if only of $\sim 10\%$ at $z \sim 22$). For what concerns the role of metal cooling at $T < 10^4$ K, in the cluster simulations we have run, fine structure transitions can actually cool the local temperature down to some 10^2 K.

REFERENCES

1. N. Yoshida, T. Abel, L. Hernquist, and N. Sugiyama, *ApJ* **592**, 645–663 (2003).
2. V. Springel, *MNRAS* **364**, 1105–1134 (2005).
3. D. Galli, and F. Palla, *A&A* **335**, 403–420 (1998).
4. P. C. Stancil, S. Lepp, and A. Dalgarno, *ApJ* **509**, 1–10 (1998).
5. D. W. Savin, *ApJ* **566**, 599–603 (2002).
6. J. G. Wang, and P. C. Stancil, *Physica Scripta*, *T96* **1**, 72–+ (2002).
7. A. Lipovka, R. Núñez-López, and V. Avila-Reese, *MNRAS* **361**, 850–854 (2005).
8. D. Hollenbach, and C. F. McKee, *ApJS* **41**, 555–592 (1979).
9. D. Hollenbach, and C. F. McKee, *ApJ* **342**, 306–336 (1989).
10. D. E. Osterbrock, *Astrophysics of gaseous nebulae and active galactic nuclei*, Research supported by the University of California, John Simon Guggenheim Memorial Foundation, University of Minnesota, et al. Mill Valley, CA, University Science Books, 1989, 422 p., 1989.
11. F. Santoro, and J. M. Shull, *ApJ* **643**, 26–37 (2006).
12. U. Maio, K. Dolag, B. Ciardi, and L. Tornatore, *MNRAS* **379**, 963–973 (2007).
13. R. S. Sutherland, and M. A. Dopita, *ApJS* **88**, 253–327 (1993).
14. U. Maio, K. Dolag, M. Meneghetti, L. Moscardini, N. Yoshida, C. Baccigalupi, M. Bartelmann, and F. Perrotta, *MNRAS* **373**, 869–878 (2006).
15. G. Tormen, F. R. Bouchet, and S. D. M. White, *MNRAS* **286**, 865–884 (1997).
16. L. Tornatore, S. Borgani, F. Matteucci, S. Recchi, and P. Tozzi, *MNRAS* **349**, L19–L24 (2004).